Progress In Electromagnetics Research C, Vol. 113, 227–238, 2021

K- and Ka-Band Planar Spiral Antenna Arrays with Integrated Corporated Feeding Network

Paul Tcheg and David Pouhè*

Abstract—Although spiral antennas have undergone continuous development and refinement since Edwin Turner conceived them in 1954, only a few compact planar arrays exist. The shortcoming is even more significant when it comes to spiral antenna arrays in mode M2 operation. The present work addresses this issue, among other things. Based on a framework recently published, the paper presents two planar arrays of spiral antennas operating in the same frequency band and radiating for the first one an axial mode M1 and a conical mode M2 for the second. Both arrays are modeled, simulated, and fed with a corporate feeding network embedded in a dielectric substrate. It is shown that keeping the same topology, the array for conical M1 mode can be obtained from the array for mode M2 by a simple introduction of a phase shift on one branch of the feed and vice versa, providing thus the possibility to obtain in the same structure a spiral antenna array operating in both modes in the same frequency band simultaneously. Comparison between simulated and measured data shows good agreement.

1. INTRODUCTION

The digital transformation of the economy and society goes hand in hand with the current megatrends of big data/cloud computing on the one hand and Industry 4.0/Internet of Things on the other hand. The future's key technology, "Artificial Intelligence," is seen as a promising and sustainable growth engine for industry and services. To enable the digital paradigm shift and ensure anyone's connectivity everywhere and at any time, a comprehensive expansion or renewal of the IT and mobile infrastructures is required. In addition to the IT networking of "man and machine," "smart objects," i.e., ubiquitous systems which communicate via interfaces, must be further developed. The simultaneous supply of the "intelligent objects" with data and communication to each other is to a great part thanks to antennas, as transitional components in the communication scheme between two RF systems, as they convey conducted electromagnetic energy into free space waves and vice versa. That is, antennas play a paramount role in the development and deployment of this technology.

Among the antenna candidates to be used in distributed ad hoc network systems, broadband antennas are the most attractive, as they ensure a high data rate in wireless communication systems. Spiral antennas are the most prominent in this class of antennas. They are not only wideband but also circularly polarized by nature. This last feature makes them immune to the Faraday rotation effect and less sensitive to fading due to polarization mismatch and interferences encountered in multipath propagation in mobile communication. Therefore, circularly polarized antennas are widely used in navigation systems and satellite communication [1, 2]. However, the drawback of spiral antennas is their low directivity when they are constructed as a planar antenna. High gain directive antennas are often needed in ubiquitous systems; this is an issue to overcome.

Received 9 April 2021, Accepted 23 June 2021, Scheduled 1 July 2021

* Corresponding author: David Pouhè (david.pouhe@reutlingen-university.de).
The authors are with the School of Engineering, Reutlingen University of Applied Sciences, Alteburgstrasse 150, D-72762 Reutlingen, Germany.

In the development of this new technology, the trend is towards small compact electronic devices. The realization of such extreme space-saving systems requires 3D packaging while taking into account the required space of passive components, which are essential parts of such systems. Reducing the area needed for passive components such as the antenna and its feeding network is an essential factor for the compactness of these systems. The design of integrated low profile compact antennas is therefore called for.

This paper addresses these issues. It presents low profile compact spiral antenna arrays which may be used in K- and Ka-bands for the 5G mobile communication systems. The array configuration is chosen to enhance the gain, while the feeding network is integrated for robustness and compactness purposes. Other feeding methods may also be possible [4].

Following these introductory words, we deal with the single element antenna structure in Section 2. Arrays designed in the frame of this work are presented in Sections 3 and 4. Linear and planar arrays for the axial mode are modeled, simulated, and analyzed in Section 3. Single element spiral antenna may also radiate in conical mode M2 [5]. For the array of spiral antennas, this may not be the case. Since mode M2 is for several applications as directional findings of interest, a 2×2 planar array for conical mode operating at the same frequencies as for its mode M1 counterpart is proposed in Section 4. In each case, simulated radiation characteristics and measured data are compared to each other. A good correlation between simulation and measurements is obtained.

Note that this work does not aim at providing a comparative study with state-of-the-art designs since measurements are sufficient to demonstrate its validity. Readers interested in any comparison with existing antennas of the same kind kindly refer to the literature [4, 6–10].

2. THE SINGLE ELEMENT ANTENNA STRUCTURE

The spiral antenna and its feed were designed and optimized based on the methodology described in [3]. Details on their design procedure will therefore not be reproduced here because of space limitation. Instead, we will only provide general aspects of their configuration along with all relevant radiation properties. For the design procedure of the radiating element and its feed, interested readers refer to [3].

Figure 1 presents the single spiral antenna element designed using ANSYS HFSS version 2018.0 and taking manufacturing requirements into consideration. It is composed of a radiating element mounted on a grounded substrate (Isola Astra MT of thickness 1.5 mm and, with a permittivity $\varepsilon_r = 3$ and dielectric losses $\tan\delta = 1.7 \cdot 10^{-3}$) to ensure the unidirectional radiation of the electromagnetic field and an integrated feeding network (Fig. 2). The spiral is an equiangular one with 0.75 turn, outer radius $\rho_{out} = 2.63$ mm, and inner radius $\rho_0 = 0.4$ mm. It exhibits a constant input impedance over a frequency band about 11.64 GHz, from 20 GHz to 31.64 GHz (Fig. 3) and overall good radiation properties in the corresponding frequency range as observed during the simulation [3].

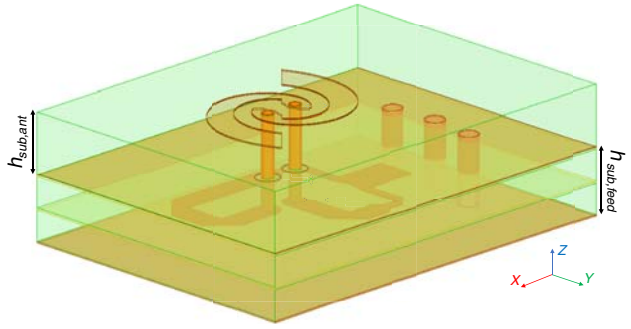

Figure 1. Single antenna element.

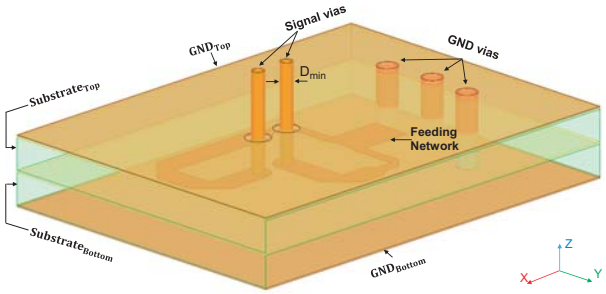

Figure 2. Feeding network (right).

The feeding network is embedded in multilayer dielectric media bounded by two conducting planes, the surrounding material, and the top and bottom metal layers to build a stripline structure in which only the principal TEM mode propagates in the frequency range of interest [3]. The dielectric material

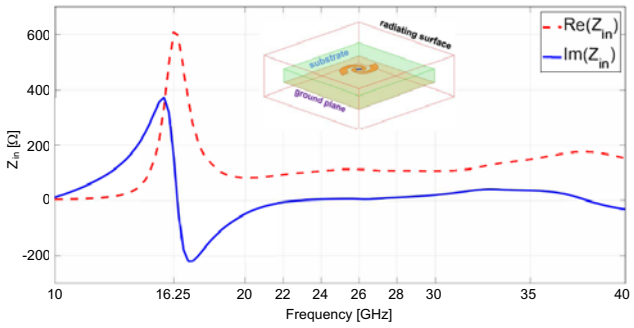

Figure 3. Input impedance curve of the radiating element when fed ideally.

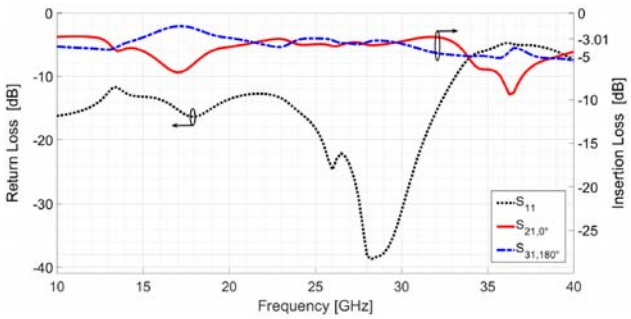

Figure 4. Input reflection coefficient and insertion loss of the feeding network.

is of the same permittivity as that on which the radiating element is mounted. Energy transfer between radiating element and feed is ensured through vertical interconnect accesses (vias), one via each arm, whose equivalent radius was obtained as:

$$r_{via} = \begin{cases} \dfrac{W_{\text{Trace}} \cdot A_s}{2\alpha\left(\dfrac{30\pi}{\sqrt{\varepsilon_r} Z_0} - 0.441\right)}, & \text{for } \sqrt{\varepsilon_r} \cdot Z_0 < 120\,\Omega \\ \dfrac{W_{\text{Trace}} \cdot A_s}{2\alpha\left(0.85 - \sqrt{1.041 - \dfrac{30\pi}{\sqrt{\varepsilon_r} Z_0}}\right)}, & \text{for } \sqrt{\varepsilon_r} \cdot Z_0 > 120\,\Omega \end{cases} \tag{1}$$

where W_{Trace} is the width of the last feeding section connected to the vias (Fig. 2); A_s is the aspect ratio of the blind via, $\alpha = h_{\text{sub,feed}}/(h_{\text{sub,feed}} + h_{\text{sub,ant}})$; ε_r is the relative permittivity of the substrate; and Z_0 is the impedance of the feed's output section line. $h_{\text{sub,feed}}$ and $h_{\text{sub,ant}}$ are respectively the feed substrate's thickness and the antenna substrate's height (Fig. 1). The aspect ratio A_s depends on manufacturing process requirements.

The characteristic impedance, Z_0, of the feeding network's output section line, and hence of the spiral antenna, is obtained upon applying Equation (8) in [3]. The rest of the feeding network was designed using the transmission line theory [11] and generally accepted microwave techniques for planar corporate feeds [12–14]. The shorting pins around the input are to reduce unwanted modes and radiation in the transverse directions to stabilize the line impedance. The feeding network shows good electrical performance as can be seen from the input reflection coefficient and transmission characteristics (Figs. 4 and 5).

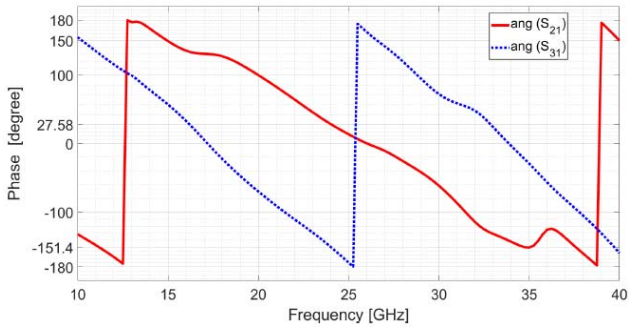

Figure 5. Phase of the feed.

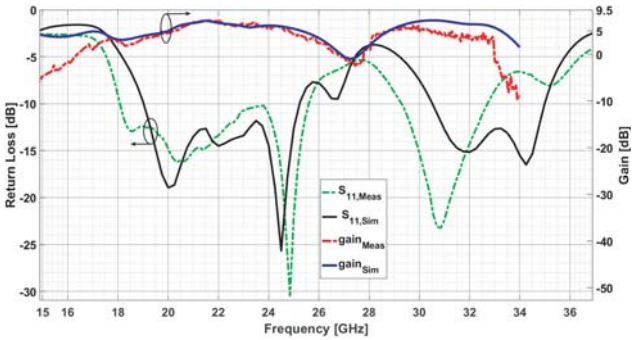

Figure 6. Reflection factor and gain of the single antenna structure.

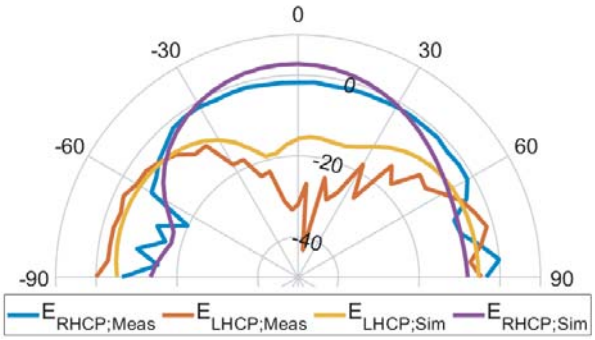

Figure 7. Co-polarization and cross-polarization components at $f = 24$ GHz.

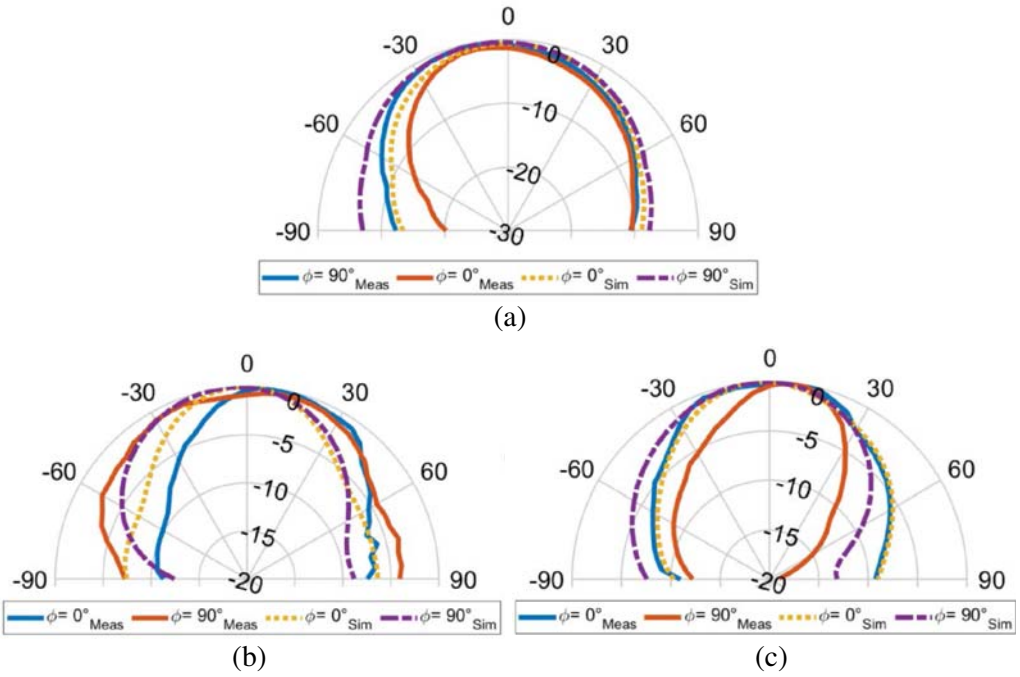

Figure 8. Radiation pattern at (a) 22 GHz, (b) 24 GHz and (c) 30 GHz of the single antenna structure.

Figures 6 to 8 display some representative results as obtained from simulations of the single antenna element structure. The antenna exhibits good radiation characteristics. For comparison, measured data have been added in Figs. 6 to 8. Experimental data were obtained throughout this work using an in-house made far-field antenna measurement system consisting of a full anechoic chamber operating from 3 to 80 GHz, a linearly polarized standard gain horn antenna, with a constant gain of 13 dB from 17 to 34 GHz, and a network analyzer (R&S ZNB). The measurement step was 50.0 MHz for frequencies and 5° for the elevation angle.

Simulated and measured results show a good correlation. The antenna has two operating bands with a 7.6 GHz impedance bandwidth from 18.1 to 25.7 GHz for the first and 3.4 GHz from 29.3 to 32.7 GHz for the second. The antenna is circularly polarized from 22.05 to 26.25 GHz, corresponding to an effective bandwidth (frequency band at which the axial ratio bandwidth matched with the impedance bandwidth [15]) of 3.51 GHz. The gain-bandwidth nearly covers the entire impedance bandwidth, with a peak gain of 7.5 dB at 22 GHz.

Co-polarization and cross-polarization components are depicted in Fig. 7 to show the direction of polarization. As can be seen, the antenna is right-hand circularly polarized (RHCP) with a high degree of polarization purity. The polarization purity is much higher for measurements than for simulation.

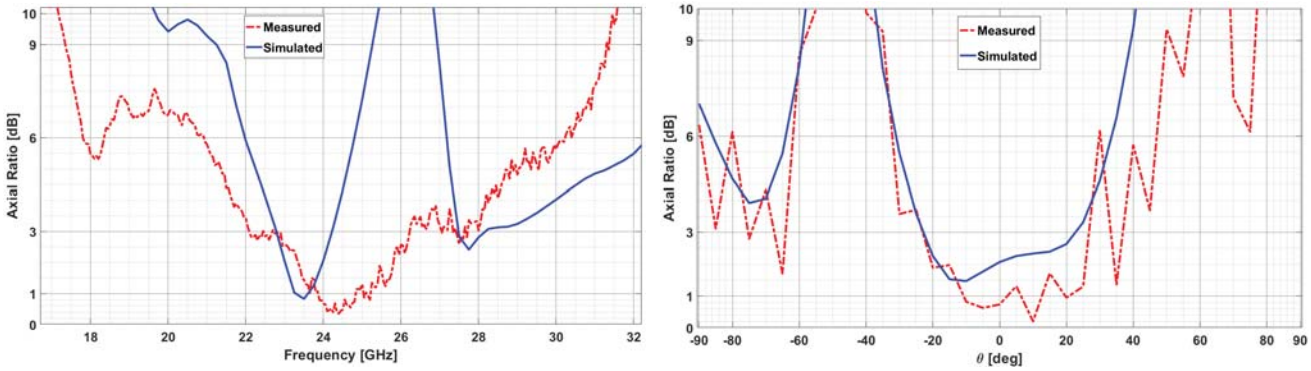

(a) (b)

Figure 9. (a) Axial ratio versus frequency and (b) as function of the elevation angle at $f = 24\,\text{GHz}$.

The cross-polar level at $\vartheta = 0°$ is 25 dB for measurement, whereas it is 19.53 dB for simulation. This purity is reflected in the axial ratio of Fig. 9 where measured and simulated data are compared to each other.

The slight discrepancies observed between measured and simulated data are discussed later in Section 3.

The antenna designed above has a relatively high gain compared to other antennas of the same size in the literature. However, for some applications, as radar systems for vehicles, where much higher performance is needed, this gain may still be insufficient. Increasing the directivity of the antenna is therefore necessary. One approach to do that is, amongst others, to increase the number of radiating elements. We deal with this issue in the next section. Prior to that, we remind that the single spiral antenna element herein designed may also operate in a second M2 mode at frequencies around 32 GHz [5]. However, this might not be the case for an array of spiral antennas†. Therefore, we will present in the following two kinds of arrays: the first for an axial M1 mode of operation and the second for the conical M2 mode.

3. ARRAYS FOR THE AXIAL MODE

Designing spiral antennas on a PCB at Super High Frequency (SHF, ITU Band) and above while maintaining the radiating device circularly polarized in the operating frequency band is a cumbersome task [16]. A two-stage strategy for the development of the array will therefore be adopted. The two-element array's conceptual design is first presented followed by the development of a 2×2-elements array, which is the principal configuration in this work.

3.1. The Linear 1×2-Array

The array herein investigated consists of identical elements arranged in a straight line (Fig. 10). A constructive adding of their contribution in the broadside direction while canceling in others is obtained by placing the elements at a $\frac{\lambda}{8}$-distance from each other. Since the input power must be subdivided amongst the outputs, two additional line sections with impedances Z_0 and Z_{01} were added between the input line and the transition towards the triplate output ports to maintain the impedance level between the input connector and all the output ports. The linear translation of vector $\mathbf{v}(0,\, d_y,\, 0)$ and the matrix $T_{\mathbf{V}}$

$$T_{\mathbf{v}} = \begin{bmatrix} 1 & 0 & 0 & 0 \\ 0 & 1 & 0 & d_y \\ 0 & 0 & 1 & 0 \\ 0 & 0 & 0 & 1 \end{bmatrix} \tag{2}$$

† This is an open issue that still needs investigations as to our knowledge the issue has not been addressed yet.

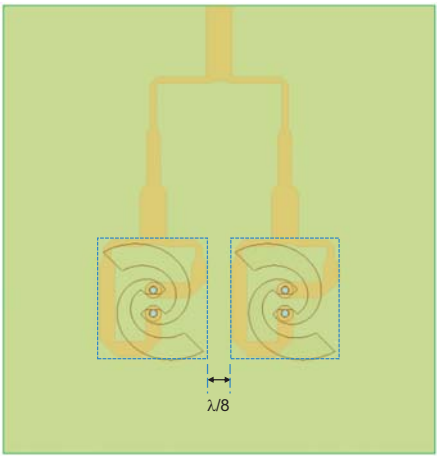

Figure 10. The 1×2 antenna for $d_y = \lambda_{eff}/8$. The structure is a representative configuration for all investigated structures.

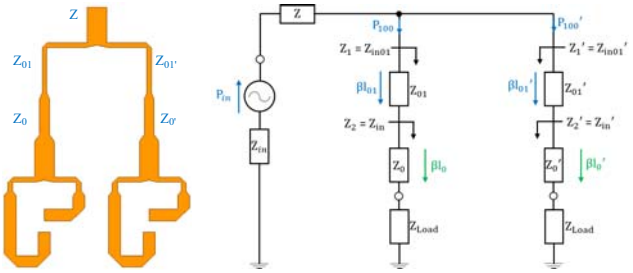

Figure 11. Feeding network for the linear array of two elements and its equivalent circuit.

whereby $d_y = \frac{\lambda}{8}$ is then applied to obtain the feeding network as displayed in Fig. 11. $\lambda/8$ was among all investigated spacing distances between the antenna elements, the distance which provided the best radiation characteristics.

Although not presented here because of space limitation, it was observed that the designed linear array of two elements shows good radiation properties at frequencies of interest. The antenna radiates an axial mode M1.

3.2. The Planar Array of 2×2-Elements

Having designed the linear array, we now turn attention to the central part of this section: the design of a planar array of spiral antennas.

The 2×2-array is easily obtained by rotating the 1×2-array by a π-angle about the z-axis, whereby the distance d_y between the elements remains unchanged. The rotation matrix is given as:

$$R_z = \begin{bmatrix} \cos\psi & -\sin\psi & 0 \\ \sin\psi & \cos\psi & 0 \\ 0 & 0 & 1 \end{bmatrix} = \begin{bmatrix} -1 & 0 & 0 \\ 0 & -1 & 0 \\ 0 & 0 & 1 \end{bmatrix} \tag{3}$$

With the given rotation, the sense of the fed energy flowing in the two lower feeding elements differs from that of the two upper ones. Unless a two-ports feeding network is intended, a phase shift of 180° shall be introduced on one branch to maintain the broadside radiation of the whole structure if a central feeding point is desired as it is the case in this work. A phase shift was therefore introduced in the lower branch. Electromagnetic coupling due to crosstalk with other feeding sections was avoided by realizing the phase shift part towards the substrate's boundaries (Fig. 12).

Figure 13 portrays the return loss and insertion loss of the designed feed. As can be seen, the feed is broadband, and the impedance bandwidth is greater than 14.5 GHz. It is well-matched at the operating frequency with a return loss value of −18 dB. Between 19.75 GHz and 28.5 GHz, the curve shows periodically increasing ripples. The period between two minima corresponds almost exactly to twice the length of the trace over which the wave propagates towards the feed arm's ends. This length is 46.6018 mm. Calculating the frequency difference between two successive minima yields $\triangle f = c_0/(\sqrt{\varepsilon_{r,eff}} \cdot 2\Delta l) = 2.27$ GHz, which almost equals the simulated value $\Delta f = 2.2$ GHz. The poor impedance matching at 25 GHz ($RL = -8.8$ dB) goes back to the superposition of reflected and incident waves at the input. Part of waves propagating from the input undergoes a reflection at the feed's arms end and travels back to the input, where they superpose both the incident field and waves reflected from the corners. To the phenomenon described here, above superposes the propagation of higher-order modes of the cavity, whose overall effect impacts the return loss.

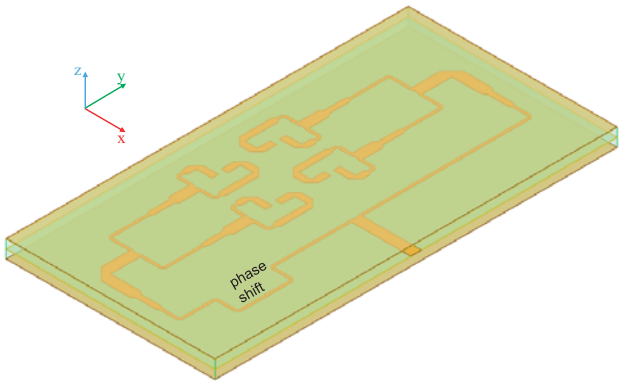

Figure 12. 3D view of the designed central feeding network.

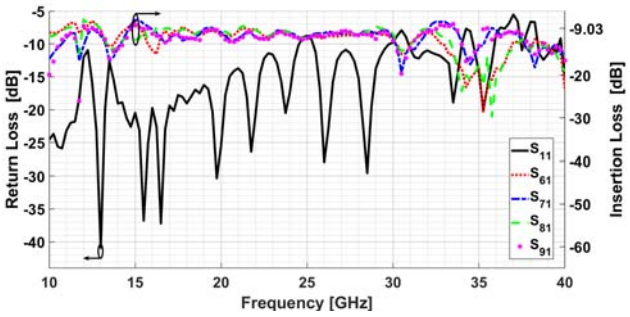

Figure 13. Return loss and insertion loss of the designed central feeding network.

At 24 GHz, the insertion loss varies between −10.6 and −9.94 dB and exhibits a constant behavior from 22.5 GHz to 29.4 GHz. This poor level of the transmission factors is due to dielectric and resistive losses and to the effect of the surface roughness on the propagation of the signal along the traces. The phase difference at output ports of each pair ranges between 178.62° and 180.95°. Interferences in the cavity are a source of this phase shift.

The final realized antenna as depicted in Fig. 14 shows good radiation characteristics (Figs. 15–18). Again, measurement data have been added to the graphs for comparison. The frequency step throughout the work is 1 GHz for simulations.

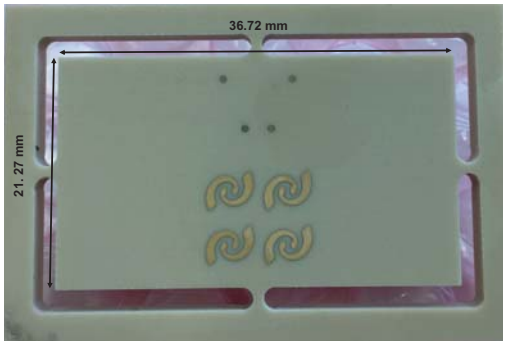

Figure 14. Final realized antenna array of four elements.

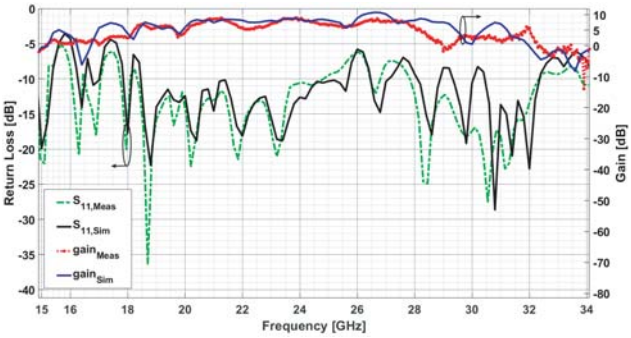

Figure 15. Return loss and gain of the planar array for the axial mode.

Sources of errors such as misalignments of the AUT in the chamber, measurement uncertainties, inaccuracies in soldering the pin connector, manufacturing tolerances, human-made noise, etc., being considered, the consistency between simulation and experiments can be well appreciated by comparing obtained results. The antenna is well matched in the K-band. As for its single element, the array shows a second operating broadband frequency window, from 27.8 to 32.4 GHz in the Ka-band. The antenna radiates circularly polarized fields at multiple frequencies between 19.5 and 30.5 GHz, corresponding to an effective bandwidth of 11 GHz. Co- and cross-polarizations in the $\varphi = 0°$- and $\varphi = 90°$-plane are displayed in Fig. 17. Despite undesired interferences appearing in measured patterns, similar trends between experimented data and simulated results are observed. At zenith, the cross-polarization level is at least −21 dB in both cut planes ($\varphi = 0°$ and 90°) at the operation frequency. The measured axial ratio versus the elevation angle shows multiple angular bandwidth windows, whereby none of the band is as large as the simulated angular bandwidth. This discrepancy between measurements and simulations in the angular bandwidth is most likely due to human-made noise and measurement uncertainties. Our

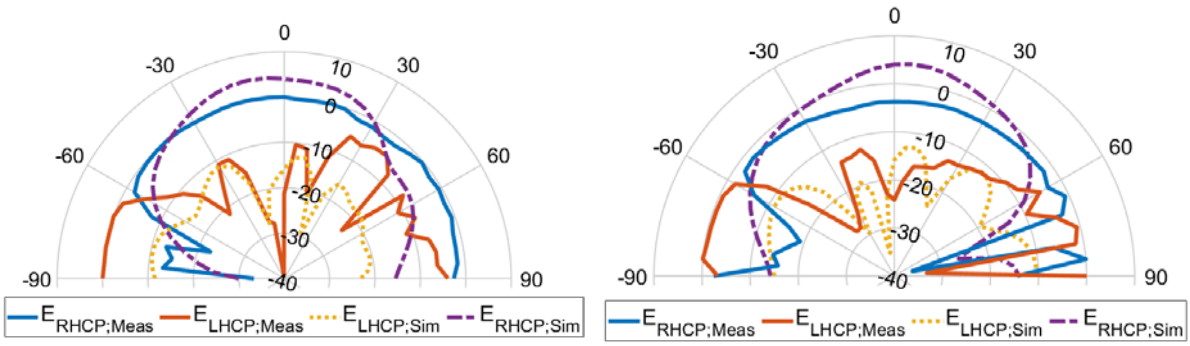

(a) (b)

Figure 16. Co- and cross-polarization components at (a) $\varphi = 0°$ and (b) at $\varphi = 90°$ of the planar array for the axial mode at $f = 24\,\text{GHz}$.

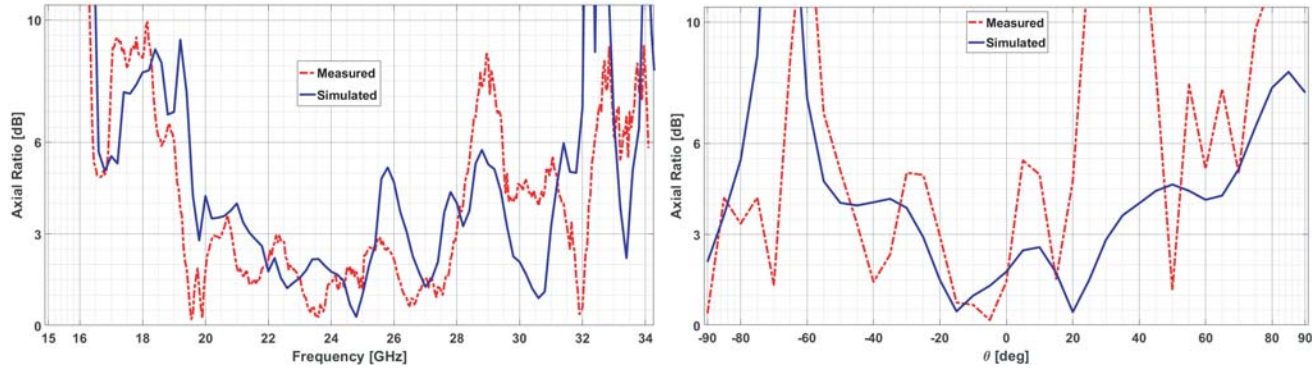

(a) (b)

Figure 17. (a) Axial ratio versus frequency and (b) as function of the elevation angle of the planar array for the axial mode.

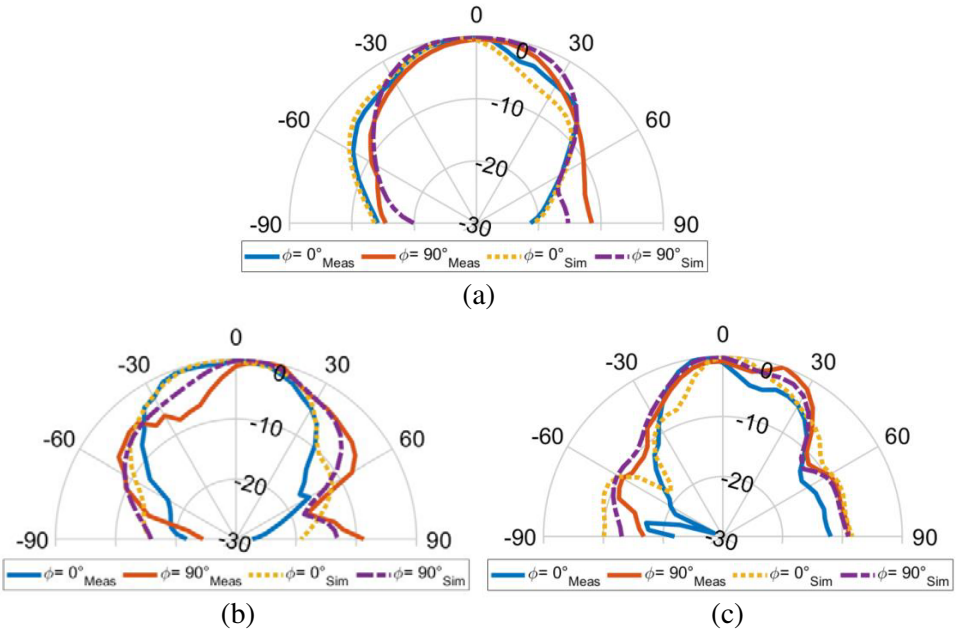

(a)

(b) (c)

Figure 18. Radiation pattern at (a) 22 GHz, (b) 24 GHz and (c) 28 GHz of the planar array for the axial mode.

measurement setup suffers from one drawback: it is not automated. The AUT is rotated manually. This fact makes angular misalignments between the transmitting and receiving antennas very likely.

From Fig. 18, it can be seen that the M1-mode remains within a large bandwith, thus showing the effectiveness of the implemented feeding network. At 28 GHz, the unique side-lobe over the large EBW appears at 65° and 75° for simulated results and experimented data, respectively.

As for the single element, the radiation diagrams of the 2 × 2-array show an asymmetry, whose causes are discussed later at the far end of the next section.

4. THE ARRAY FOR THE CONICAL MODE

The array for the conical mode has the same topology as its axial mode counterpart. The difference between the two resides in the phase shift on one branch of the feed. By removing the phase shift in the feed of Fig. 12, the antenna elements are fed by two waves with zero phase difference. Consequently, the bottom and top elements of the upper and lower pairs have the same progressive phase. The phase difference between the bottom and top elements as well as between the top and bottom elements of the upper and lower pairs respectively is 0° or 360° (Fig. 19). The antenna's polarization sense does not

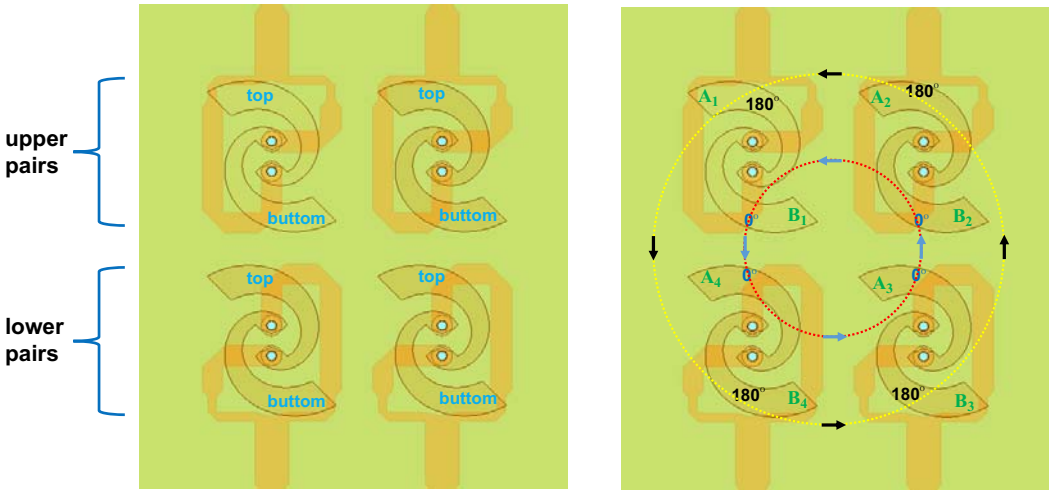

(a) (b)

Figure 19. (a) Representation of 2 × 2 conical array as pair of radiating elements and (b) illustration of the phase progression between the elements.

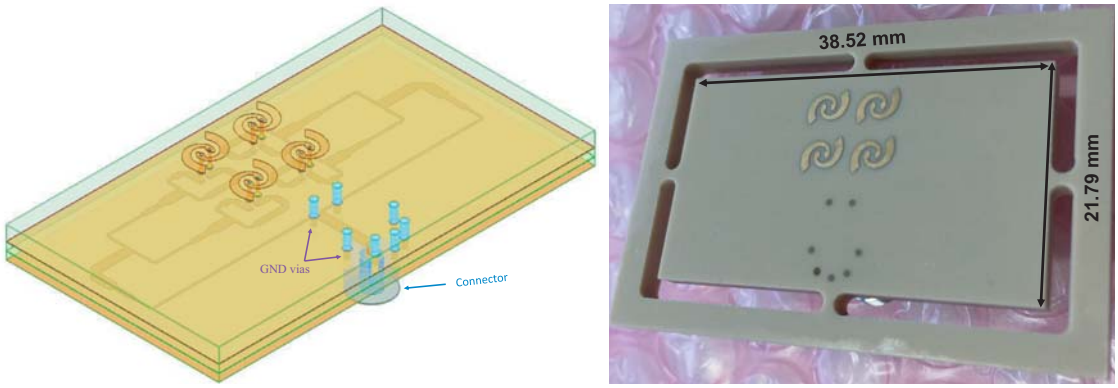

Figure 20. Structure and photograph of the fabricated planar array for conical mode.

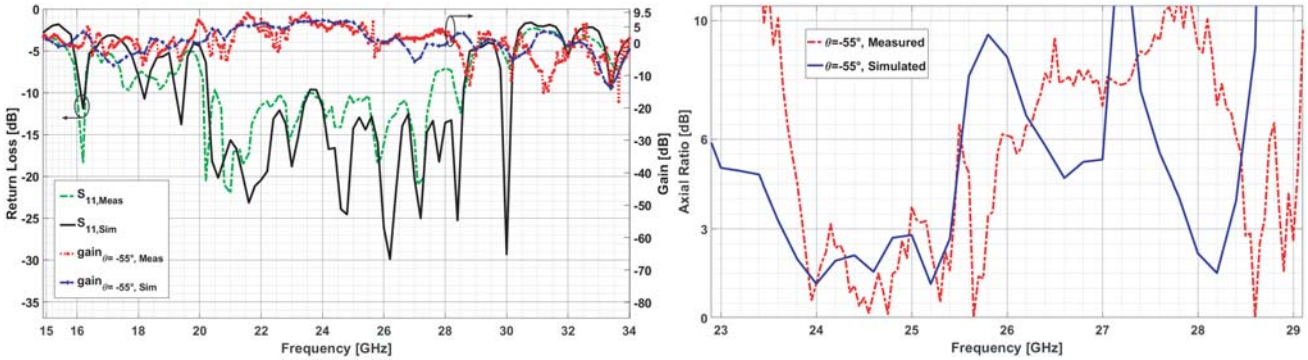

(a) (b)

Figure 21. (a) Return loss and gain, (b) axial ratio over the frequency of the planar spiral array for conial mode.

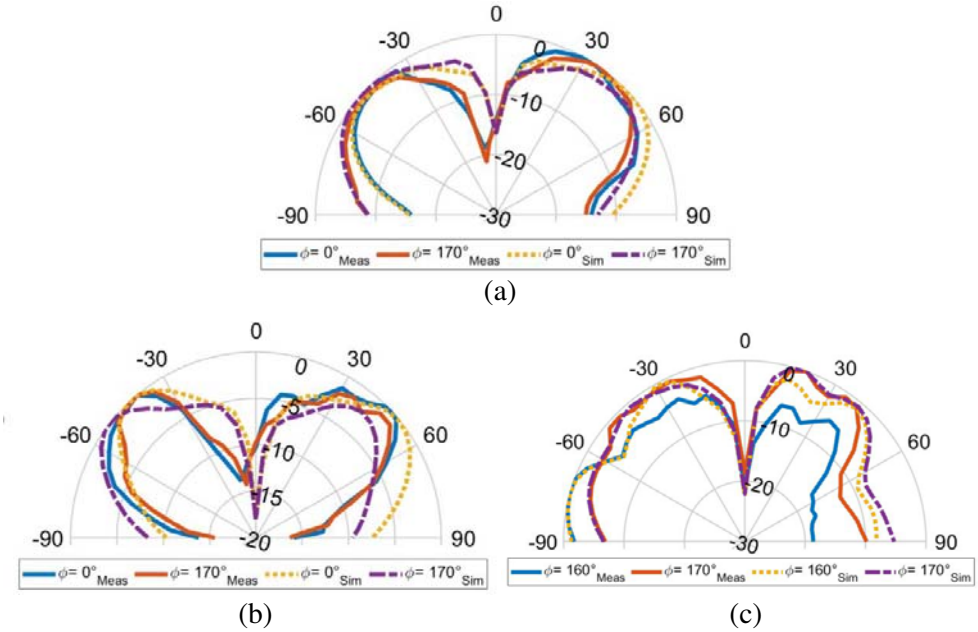

(a) (b) (c)

Figure 22. Radiation pattern at (a) 22 GHz, (b) 24 GHz and (c) 28 GHz of the planar spiral array for conial mode.

change since the spiral's winding sense defines its sense of polarization. It means that the antenna is still RHC polarized. Only the angles at which the antenna exhibits circular polarization change.

Figure 20 presents the structure and a photograph of the final realized antenna. Radiation characteristics such as the return loss, gain, axial ratio, and radiation pattern are depicted in Figs. 21 to 22. Here too, the antenna shows good radiation properties. As expected, the radiation is conical with nearly 35°-half-power beamwidth, from $-70°$ to $-37°$ and 23 to 60° at $\varphi = 170°$. At 22 GHz and 24 GHz, the null occurs at about 5°, and the broadside null gains are respectively -20 dB and -14.8 dB. In contrast, the pattern is well aligned at 28 GHz. The antenna has 7.5 GHz impedance bandwidth and an effective bandwidth of 1.8 GHz (from 23.65 to 25.45 GHz) at $\vartheta = 55°$ and $\varphi = 170°$. This bandwidth encloses frequencies at which the antenna shows a gain above 5 dB. The gain is above 5 dB over 3.9 GHz frequency band, from 21.3 to 25.2 GHz, with a maximum of 7.4 dB at 23.6 GHz. Again, as expected, measurements and simulations correlate well. Observed discrepancies are due to the same reasons mentioned above in Section 2.

In quasi, all radiation patterns, those for mode M1 and mode M2 as well, an asymmetry is noticeable

and even conspicuous at high frequencies. This asymmetry goes back to

1) - the asymmetrical arrangement of the radiating elements with respect to the y-axis,
2) - the influence of the substrate,
3) - the cumulative scattering effects of the ground and spurious emission of the waveguide made up of the two conducting planes (top and bottom metal layers) and the substrates surrounding the feeding network.

Part of the energy coupled at the input excites waves (guide- and surface-waves) within the waveguide. Despite the existence of shorting pins around the input to reduce unwanted modes and radiation in the transverse directions and, to stabilize the line impedance, part of these waves propagate along the line and radiate at the interface substrate-air. This radiation, which, because of the enlargement of the PCB and the subsequent asymmetrical position of the input, is most pronounced at the boundary site close to the input port, superposes the spiral elements' radiation and gives rise to asymmetry in the pattern (Fig. 23).

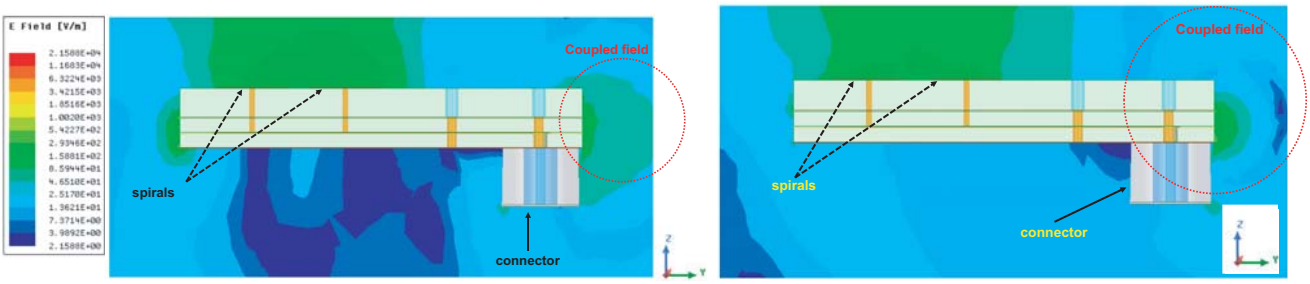

Figure 23. Spurious emission given rise to asymmetry in the pattern.

5. CONCLUSION

Based on a framework recently published, two compact planar arrays of spiral antennas with an integrated feed operating in mode M1 and mode M2 respectively have been designed and investigated. The antenna radiating elements have a small number of turns compared to conventional spirals. It is shown that keeping the same topology, the array for conical M2 mode can be obtained from the array for mode M1 by a simple introduction of a phase shift on one branch of the feed and vice versa. Providing thus the possibility to obtain in the same structure a spiral antenna array operates in both modes in the same frequency band simultaneously. The antennas are of overall good radiation characteristics, despite an asymmetry in the radiation pattern. This asymmetry is mainly due to spurious radiation of the waveguide made up of the two conducting planes and the feeding network substrates. Simulated and measured data agree well. A multiple-inputs solution may provide much compact antenna arrays with symmetrical radiation patterns; however, at a high production cost. This is an issue that will be addressed in a paper to come.

The antennas herein proposed are for K- and Ka-bands. Nevertheless, because of the Maxwell equations' linearity, the approach used for their design can be applied at higher frequencies provided that relevant EMC and signal integrity issues that may appear are tackled.

REFERENCES

1. Lai, H. W., D. Xue, H. Wong, K. K. So, and X. Y. Zhang, "Broadband circularly polarized patch antenna arrays with multiple-layers structure," *IEEE Antennas and Wireless Propagation Letters*, Vol. 16, 525–528, 2016.
2. Karlson, C., P. Cavero, T. Tekin, and D. Pouhè, "A new broadband antenna for satellite communications," *Antennas & Propagation in Wireless Communications*, 2014.

3. Tcheg, P. and D. Pouhè, "A design methodology for the implementation of planar spiral antennas with an integrated corporate feed," *Progress In Electromagnetics Research C*, Vol. 106, 239–253, 2020.
4. Baghernia, E., M. M. Ali, and A. R. Sebak, "2 × 2 slot spiral cavity backed antenna array fed by printed gap waveguide," *IEEE Access*, Vol. 8, 170609–170617, 2020.
5. Duhamel, R. H. and J. P. Scherer, "Frequency independant antenna," *Antenna Engineering Handbook*, R. C. Johnson, McGraw-Hill, New York, 1993.
6. Zhou, H., A. Pal, A. Mehta, and H. Nakano, "6 × 6 array of four-arm spiral antennas for high-gain satellite receiver applications at low elevation," *Proc. 2018 IEEE Int. Symp. on Antennas and Propagation & USNC/URSI National Radio Science Meeting*, 469–470, Jul. 8–13, 2018.
7. Zhu, Q., K.-B. Ng, and C. H. Chan, "Printed circularly polarized spiral antenna array for millimeter-wave applications," *IEEE Trans. Antennas and Propagation*, Vol. 65, No. 2, 636–643, Feb. 2017.
8. Huang, J., W. Lin, F. Qiu, C. Jiang, D. Lei, and Y. J. Guo, "A low profile, ultra-lightweight, high efficient circularly-polarized antenna array for Ku band satellite applications," *IEEE Access*, Vol. 5, 18356–18365, 2017.
9. Wu, Q., J. Hirokawa, J. Yin, C. Yu, H. Wang, and W. Hong, "Millimeter-wave planar broadband circularly polarized antenna array using stacked curl elements," *IEEE Trans. Antennas and Propagation*, Vol. 65, No. 12, 7052–7062, Dec. 2017.
10. Baghernia, E., R. Movahedinia, and A. R. Sebak, "Broadband compact circularly polarized spiral antenna array fed by printed gap waveguide for millimeter-wave applications," *IEEE Access*, Vol. 9, 86–95, 2021.
11. Pozar, D. M., *Microwave Engineering*, 4th Edition, John Wiley & Sons, New York, 2012.
12. Henderson, A. and J. R. James, "Design of microstrip antenna feeds. Part 1: Estimation of radiation loss and design implications," *IEE Proc. H — Microwaves, Optics and Antennas*, Vol. 128, No. 1, Feb. 1981.
13. Hall, P. S. and J. R. James, "Design of microstrip antenna feeds. Part 2: Design and performance limitations of triplate corporate feeds," *IEE Proc. H — Microwaves, Optics and Antennas*, Vol. 128, No. 1, Feb. 1981.
14. Horng, T. S. and N. G. Alexopoulos, "Corporate feed design for microstrip arrays," *IEEE Trans. Antennas and Propagation*, Vol. 41, No. 12, 1615–1624, Dec. 1993.
15. Tcheg, P., K. D. Bello, and D. Pouhè, "A planar equiangular spiral antenna array for the V-/W-band," *Proc. 11th European Conference on Antennas and Propagation (EUCAP)*, 1148–1152, Mar. 19–24, 2017.
16. Chen, T.-K., "Analysis and design of a multifunctional spiral antenna," Dissertation, Texas A&M University, Aug. 2012.